Astron. Astrophys. 325, 124–134 (1997)

ASTRONOMY
AND
ASTROPHYSICS

The interstellar medium in the edge-on galaxy NGC 5907

Cold dust and molecular line emission

M. Dumke[1], **J. Braine**[2,3], **M. Krause**[1], **R. Zylka**[1], **R. Wielebinski**[1], **and M. Guélin**[3]

[1] Max-Planck-Institut für Radioastronomie, Auf dem Hügel 69, D-53121 Bonn, Germany
[2] Observatoire de Bordeaux, URA 352, CNRS/INSU, B.P. 89, F-33270 Floirac, France
[3] Institut de Radioastronomie Millimétrique, 300 rue de la Piscine, F-38406 St. Martin d'Hères, France

Received 17 February 1997 / Accepted 18 March 1997

Abstract. In this paper we present new observations of the interstellar medium in the non-interacting edge-on galaxy NGC 5907. We have observed the $J = 2 - 1$ and $J = 1 - 0$ lines of the ^{12}CO molecule and radio continuum emission at λ 1.2 mm.

The distribution of the molecular gas (as traced by CO) shows a maximum in the central region and a ring or spiral arm at $r \sim 7$ kpc. Further analysis of the major axis distribution reveals evidence for an inner ring-like structure at $r \sim 3.5$ kpc. The kinematics can be described by rigid rotation in the inner part, a turnover at ~ 3 kpc, and differential rotation with a velocity of 230 km/s in the outer disk.

The observed continuum emission is mainly due to thermal radiation of cold dust with an average temperature of $T_{\rm d} = 18$ K, with a small gradient from 20 K to 16 K from the centre to the outer disk. This cold dust component is necessary to explain our results.

The dust emission closely follows the molecular gas in the central region, but is also detected at large radii where no CO can be seen. In these regions the dust absorption cross section per H atom at λ1.2 mm is estimated to be $\sigma_\lambda^{\rm HI} \sim 4.5\,10^{-27}$ cm^2, a value similar to that in the outer parts of other galaxies.

From the λ1.2 mm emission we estimated a molecular mass of NGC 5907 of 0.9 10^9 M$_\odot$, about 50 % smaller than from the CO emission. By combining the CO and continuum data we found that the CO-H_2-conversion ratio increases with galactocentric radius, from $\sim$ 0.7 10^{20} at the centre to $\sim 1.6\,10^{20}$ cm^{-2}/K km s^{-1} at $r = 7.5$ kpc.

A comparison of NGC 5907 and other edge-on galaxies concerning gas distribution, central kinematics and dust properties is presented.

Key words: galaxies: individual: NGC 5907 – galaxies: ISM – galaxies: kinematics and dynamics – infrared: galaxies – radio continuum: galaxies – radio lines: galaxies

Send offprint requests to: M.D. (mdumke@mpifr-bonn.mpg.de)

1. Introduction

The evolution of spiral galaxies and their properties are determined by many processes. One of the most important points is the occurrence and time-scale of star formation, which depends mainly on the amount, composition, and distribution of the available raw material. This raw material consists of neutral gas in either atomic or molecular form.

The amount of atomic hydrogen can easily be derived from measurements of the 21 cm line of HI. The mass of molecular hydrogen, on the other hand, is usually determined indirectly by observing the lowest rotational transition of the CO molecule. The measured line intensities are converted into H_2 column densities using a conversion factor $X = N_{\rm H2}/I_{\rm CO(1-0)}$. The estimated molecular mass, however, is quite uncertain because X is still a matter of debate (e.g. Maloney & Black 1988; Combes 1991; Arimoto et al. 1996).

Observations of thermal dust emission at mm-wavelengths provide an alternative way to estimate the total mass of the interstellar matter of a spiral galaxy. Although this emission is difficult to observe due to its weakness, it has several advantages. Firstly, at millimeter wavelengths the dust is optically thin. Secondly, the emission scales roughly with the first power of the temperature. Thirdly, at this wavelength the dust absorption cross sections do not depend very much on physical dust properties like grain size, shape, composition, and surface properties (Hildebrand 1983; Draine & Lee 1984). And, finally, interstellar dust is about 2 orders of magnitude more abundant than the most abundant CO molecule in normal spiral galaxies.

In the last few years, the advent of multi-channel bolometer arrays has made it possible to obtain high quality maps (i.e. high angular resolution and high sensitivity) of the cold dust emission of nearby spiral galaxies. In order to study the relation of the dust to the atomic and molecular hydrogen in a normal late-type spiral, we decided to observe the non-interacting edge-on galaxy NGC 5907.

This galaxy shows a relatively low level of star formation from the weak infrared emission measured by IRAS (Young et

al. 1989). Therefore it is – together with NGC 4565 observed by Neininger et al. (1996) – some kind of counterpart to the more active galaxies already observed in the radio continuum at mm-wavelengths: NGC 891 (Guélin et al. 1993), NGC 3079 (Braine et al. 1997), NGC 3627 (Sievers et al. 1994), NGC 4631 (Braine et al. 1995), and M 51 (Guélin et al. 1995).

NGC 5907 was observed in the HI-line twenty years ago and was the first non-interacting galaxy where a galactic warp could be detected (Guélin et al. 1974; Sancisi 1976). Former CO measurements (Sofue 1994; García-Burillo & Guélin 1995) have shown that this galaxy is relatively weak in CO. Although its nearly edge-on orientation of $i \sim 86\overset{\circ}{.}5$ does not allow us to observe the emission of individual star forming regions or spiral arms in the disk, this inclination increases the column density along the line of sight to a significant and easier measurable value. Therefore NGC 5907 is a good candidate to study the radial distribution of the dust and its correlation with the molecular and atomic hydrogen distributions. This will be done especially in comparison with the other non-interacting edge-on galaxies mentioned above, namely NGC 891 and NGC 4565. The latter one shows an even lower star formation activity than NGC 5907 and is also CO-weak, whereas NGC 891 contains a considerable amount of molecular gas and shows a relatively high level of star formation. These two galaxies are classified as Sb and Sbc, respectively, in contrast to the Sc-galaxy NGC 5907.

Furthermore edge-on galaxies are suitable to investigate the thickness of the gas and dust layer. Since NGC 5907 is lacking strong star formation, one does not expect to detect a thick disk or halo in this galaxy because star formation and the existence and structure of a gaseous halo seem to be directly connected (e.g. Dahlem et al. 1995).

In this paper we present our molecular line and bolometer observations of NGC 5907. The following section describes the observations and the data reduction. Sect. 3 presents the results we obtained from the CO observations. In Sect. 4 we discuss the thermal dust emission. We estimate dust temperatures and absorption cross sections, and compare the distribution of the cold dust with that of the atomic and molecular gas. From this we get some hints on how the CO-H_2-conversion factor may vary in galactic disks. In Sect. 5 the results for NGC 5907 are compared with those obtained for other edge-on galaxies, and the final section gives a summary of our results and some concluding remarks.

Table 1 lists some basic parameters of NGC 5907 which will be used throughout this paper.

Table 1. Some basic parameters of NGC 5907

Type	Sc	(de Vaucouleurs et al. 1991)
λ1.2 mm centre:		(this work)
R.A. [1950]	$15^{\rm h}14^{\rm m}35\overset{\rm s}{.}7$	
Dec. [1950]	$56^\circ30'37\overset{''}{.}0$	
Dynamical centre:		(García-Burillo et al. 1997)
R.A. [1950]	$15^{\rm h}14^{\rm m}35\overset{\rm s}{.}5$	
Dec. [1950]	$56^\circ30'43\overset{''}{.}3$	
$v_{\rm hel}$	677 km/s	(García-Burillo et al. 1997)
Distance	11 Mpc	(Sasaki 1987)
	($1''$ corresponds to 53 pc)	
Pos. Angle	155°	(Barnaby & Thronson 1992)
Incl.	86.5°	(García-Burillo et al. 1997)

2. Observations and data reduction

The observations presented here were all made with the 30 m telescope of the Institut de Radio Astronomie Millimétrique (IRAM), located on Pico Veleta (Spain).

2.1. Molecular line observations

The observations of the ^{12}CO$(1-0)$ and the ^{12}CO$(2-1)$ lines were done in May 1995 and July 1996. We used one 3 mm (two during the second observing period) and two 1 mm SIS receivers available at the 30 m telescope simultaneously. The receivers were tuned for image sideband rejections $\geq$ 10 dB ($\geq$ 30 dB at 115 GHz). The system temperatures were 300 - 400 K at 115 GHz and 500 - 700 K at 230 GHz (in the $T_{\rm A}^*$ scale). In the following we use main-beam line brightness temperatures $T_{\rm mb}$. These are converted from the antenna temperatures, corrected for atmospheric attenuation and rear spillover, $T_{\rm A}^*$, through $T_{\rm mb} = T_{\rm A}^*/\eta_{\rm mb}$. The beam efficiencies $\eta_{\rm mb} = B_{\rm eff}/F_{\rm eff}$ are 0.73 and 0.45 for 115 and 230 GHz, respectively. The beamwidth was measured on Mars to be $21''$ for the ^{12}CO$(1-0)$ line and $11''$ for the ^{12}CO$(2-1)$ line. The backends used consisted of two 512×1 MHz channel filter banks, connected to one 3 mm and one 1 mm receiver, and an autocorrelator unit, connected to the other 1 mm receiver (and the other 3 mm receiver in July 1996).

The observations were centered on the major axis of the galaxy. Adopting the central position from the bolometer observations (given in Table 1), we observed several points out to a projected radius of $240''$ with $12''$ spacings near the centre and $24''$ spacings further out. Additionally we observed a few points above and below the major axis at distances of $12''$ and $24''$ from the plane. The observations were made by wobbling the subreflector at a rate of 0.5 Hz between the source and a reference position located between $\pm 2'$ and $\pm 4'$ in azimuth (depending on the observing position and the orientation of the source). Some scans at larger radii were observed in the position-switching mode with on- and off-position located symmetrically around the center. Cold load calibrations were made every 4 - 8 minutes.

During the CO observations we checked the pointing accuracy in two different ways. Firstly, we made pointing scans towards 1641+399 and 1418+546 every 1 - 2 hours. Secondly, we measured (every $\sim$ 2 hours) small cuts perpendicular to the major axis at the center, consisting of three points at $z = 0'', +12'',$ and $-12''$, and checked their symmetry, since the central point is expected to be strongest and the intensity of both off-axis points to be roughly equal. From these cuts and the pointing corrections made after each pointing scan we conclude that the mean pointing uncertainty is $\sim 1\overset{''}{.}5$.

The data reduction was done in a standard manner using the GILDAS software package.

2.2. Bolometer observations

The $\lambda 1.2$ mm observations were carried out in March 1995 with the 19-channel bolometer array developed at the Max-Planck-Institut für Radioastronomie, Bonn. The 19 channels are located in the centre and on the sides of two concentric regular hexagons, with a spacing between two adjacent channels (beams) of $20''$. The central frequency and bandwidth of the bolometer are estimated to be 245 GHz and 70 GHz respectively (Guélin et al. 1995). For calibration purposes we have observed maps of Mars and Uranus during the bolometer observations. These maps yielded a conversion factor from observed counts to mJy/beam area of 0.32 mJy (beam area)$^{-1}$ count^{-1}. The beamwidth at this frequency is $\sim 10''.7$.

The continuum maps of NGC 5907 were observed in the Az-El coordinate system, with a scanning speed of $4''$/s in Azimuth with data-acquisition every $2''$, and a subscan separation of $4''$ in elevation. During the observations, the subreflector was wobbled at 2 Hz in azimuth, with a beam throw of $1'$. The starting point of each subscan was shifted a few arcseconds in azimuth with respect to the preceding one, which leads to a skewed shape of each single coverage in the Az-El space, with two edges of the maps parallel to the major axis of the galaxy. This as well as the use of different map sizes (between $330'' \times 100''$ and $250'' \times 180''$) was done in order to ensure that each subscan covers the galaxy and at least $90''$ of blank sky on either side. We observed a total of fifteen single maps of NGC 5907, five centered on the optical centre (Barnaby & Thronson 1992), the others shifted $164''$ along the major axis to the northwest and southeast, respectively. Since the optical centre and the centre of the $\lambda 1.2$ mm emission (as found by our observations) differ by a few arcseconds, all offsets throughout this paper are relative to the latter position which is given in Table 1.

During the bolometer observing session the pointing accuracy was checked every 1 - 2 hours on 1418+546. The pointing corrections were always smaller than $3''$. The atmosphere was relatively stable and the sky opacity was ~ 0.2 most of the time (always smaller than 0.3). NGC 5907 was observed at relatively high elevations (55° - 70°) what reduces possible calibration errors, which are typically of the order 15 %.

The data reduction was done with the MOPS software. A second order baseline was fitted to each individual scan in azimuth direction. The final restoration was done applying the "mask-and-shift" restoring method, as outlined in the "Pocket Cookbook" (Zylka 1996).

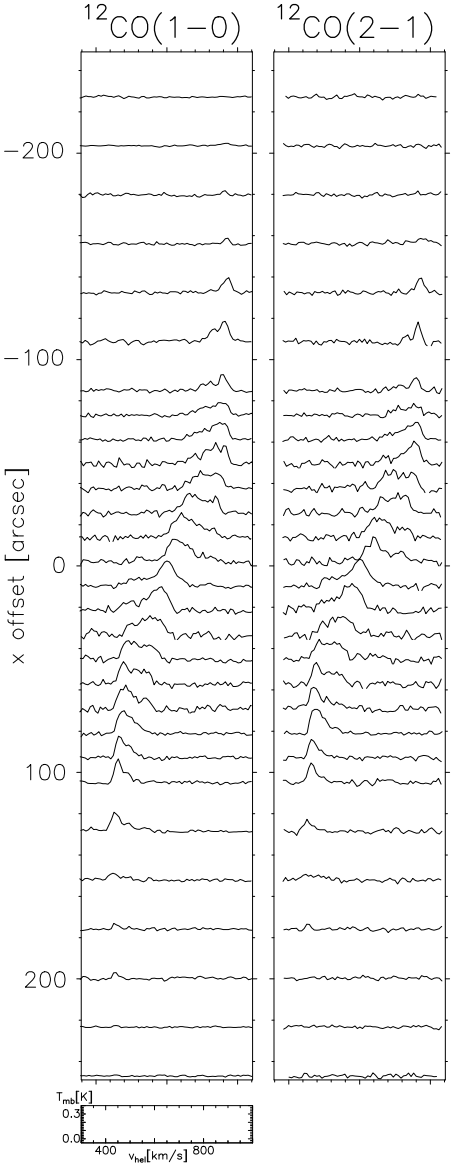

Fig. 1. Maps of the observed ^{12}CO(1 − 0) (left) and ^{12}CO(2 − 1) (right) major axis spectra of NGC 5907, smoothed to a velocity resolution of 10.4 km/s. The scale of the spectra is indicated by the small box at the bottom. Offsets are along the major axis, north is negative

3. Molecular gas in NGC 5907

3.1. Observational results and kinematics

The spectra along the major axis of the galaxy obtained during the molecular line observations are shown in Fig. 1. The maximum peak temperatures of $\sim$ 0.33 K and $\sim$ 0.36 K for the CO(1 − 0) and the (2 − 1) line respectively are reached near the center. CO is detected up to radii of more than $200''$ ($\sim$ 11 kpc).

A striking feature of many of the spectra ($r \leq 80''$) is that the observed lines contain at least two components, and that the central spectrum shows a clear asymmetry. A natural explanation for the latter is that the location of the dynamical centre of the galaxy is not at $x = 0''$ (the centre of the $\lambda 1.2$ mm emission), but shifted by a few arcseconds to the northwest. This idea is also supported by the small asymmetry visible in the position-velocity diagrams (Fig. 2). García-Burillo et al. (1997), who observed the central region of NGC 5907 using the Plateau de Bure interferometer, found the dynamical centre of the galaxy at $\alpha_{1950} = 15^{\rm h}14^{\rm m}35^{\rm s}.5$, $\delta_{1950} = 56°30'43''.3$. This corresponds to $(x, z) = (-6''.4, +1''.2)$ in our coordinates. They also found a small offset between the dynamical centre of the galaxy and the

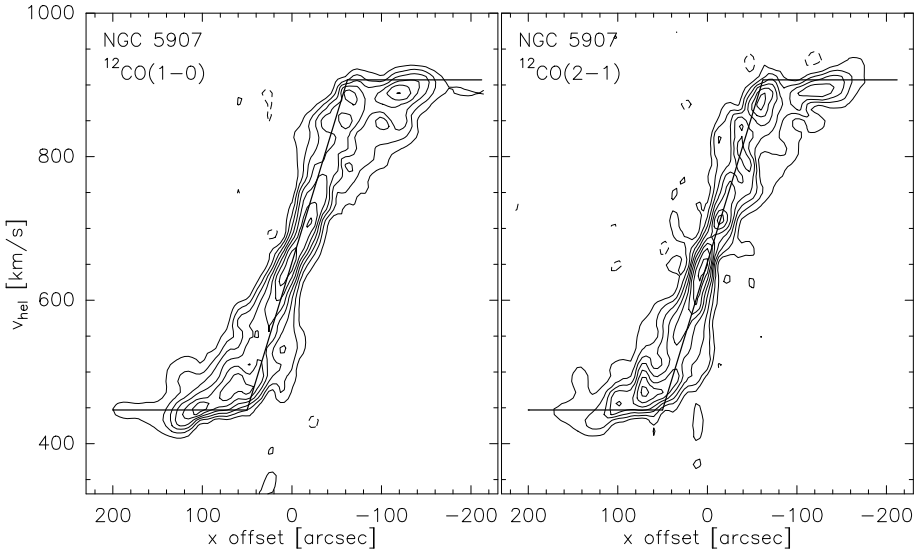

Fig. 2. Position-velocity diagram of the ^{12}CO$(1-0)$ (left) and the ^{12}CO$(2-1)$ (right) observations parallel to the major axis at $z = 0$. Contour levels are -0.04 (dashed), 0.04, 0.08, 0.12, ..., 0.4 K for both transitions. The velocity resolution is 20 km/s. The rms noise is variable along the major axis with a typical value of about 30 mK for both transitions. The thick lines indicate the rotation curve as described in the text

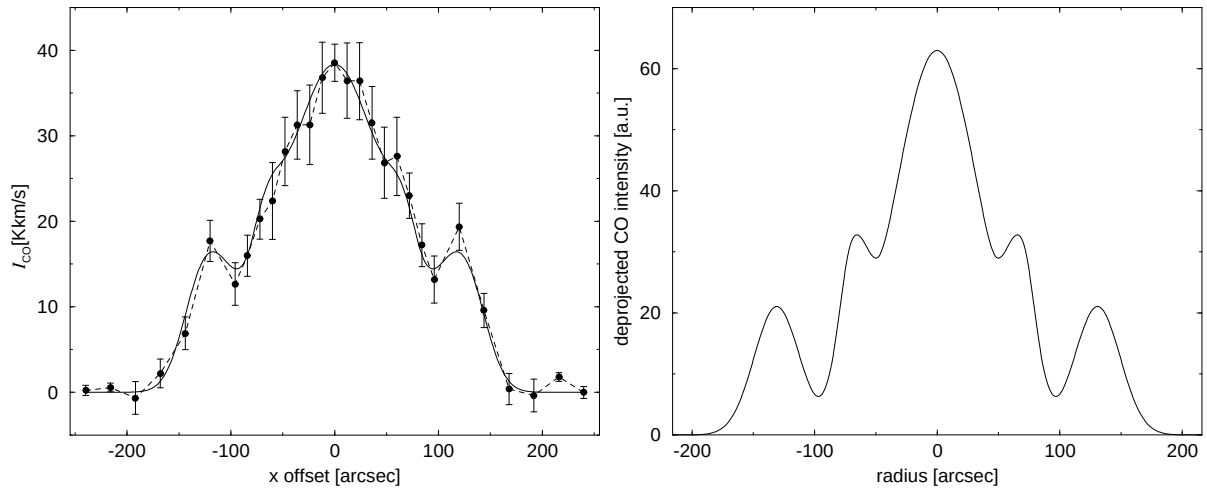

Fig. 3. a Observed (dashed line and filled black circles) and modelled (solid line) ^{12}CO$(1-0)$ intensity distribution along the major axis of NGC 5907. The modelled distribution is obtained by a least-squares-fit and results from the line-of-sight-integrated radial distribution shown in **b**. **b** Adopted radial CO profile which leads to the major axis distribution as shown in **a**

position of the maximum CO intensity, which is in agreement with our results.

The kinematics of NGC 5907 can basically be described by rigid rotation up to a radius of $\sim 55''$ (which corresponds to ~ 3 kpc), followed by differential rotation with a rotational velocity of 230 km/s. These values are relative to the systemic velocity of 677 km/s and the dynamical centre given in Tab. 1. The rotation curve follows from this work and the HI data (Casertano 1983) and is plotted as a thick line on the position-velocity diagrams (Fig. 2). There are, however, a few deviations from this simple behaviour. A second line component is visible in the spectra near the central region (at $|x| < 30''$). Here the rigid ("normal") rotation of the inner disk is accompanied by a high-velocity wing, with a much larger velocity gradient. This component is visible in the individual spectra as well as in the p-v-diagrams, and leads to a total line width of about 350 km/s at the assumed central position. It most probably results from non-circular motions due to a bar, as already suggested by García-Burillo & Guélin (1995) and García-Burillo et al. (1997).

3.2. Radial gas distribution

The observed major axis distribution of the CO intensity is the sum of the radial distribution and a projection effect (by which the emission at several radii is projected onto a certain position on the major axis). In order to deproject this distribution, we assumed a radial model function, consisting of a central Gaussian peak and two Gaussian rings, and fitted the resulting major axis distribution to the data. The existence of two ring-like structures is suggested by two intensity maxima (at $x \sim \pm 60''$ and $x \sim \pm 120''$) on either side of the centre in the p-v-diagrams.

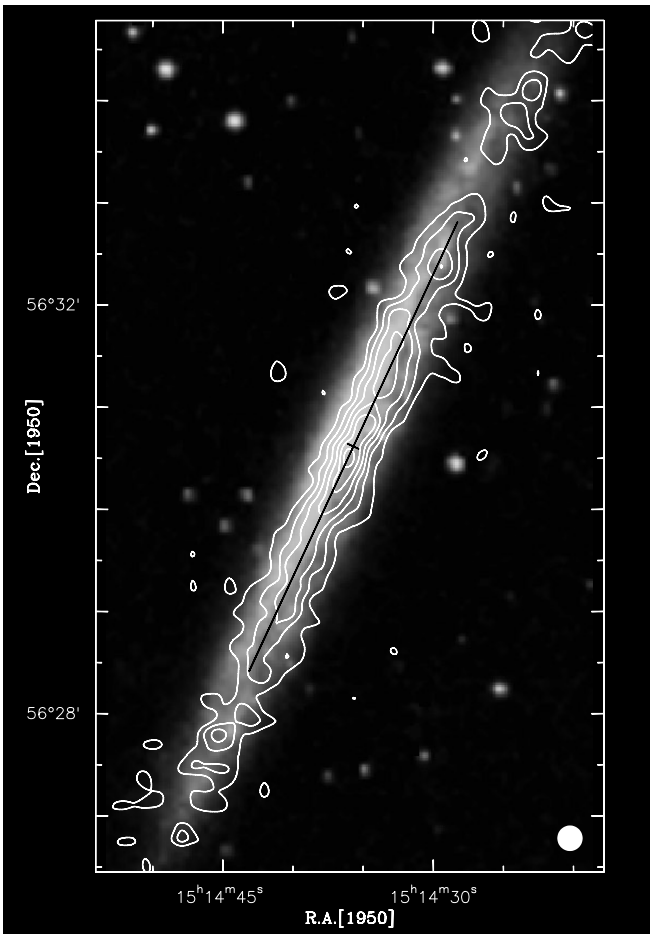

Fig. 4. Contour map of the continuum emission of NGC 5907 at 245 GHz, overlaid onto an optical image extracted from the Digitized Sky Survey. The beam size of 15″ is indicated by the filled white circle in the lower right corner. The rms noise depends on the location in the map; on the galaxy it is about 1.5 mJy/beam area, contour levels are 4, 8, . . . , 24 mJy/beam area. The thin black lines indicate the λ1.2 mm centre and the major axis of the galaxy as given in Table 1

Additionally this distribution with two rings fits the data better than a distribution with just one ring (at $r \sim 120''$).

The result can be seen in Fig. 3. The best fit was obtained for ring radii of r_1 = 3.7 kpc and r_2 = 7.0 kpc and widths (FWHM) of $\Theta_{\rm peak}$ = 4.4 kpc, $\Theta_{\rm ring1}$ = 1.4 kpc, and $\Theta_{\rm ring2}$ = 2.3 kpc for the central peak and the inner and outer ring respectively. However, the outer "ring" may in fact be spiral arms seen more or less tangentially.

4. Cold dust in NGC 5907

4.1. Observational results

A contour map of the λ1.2 mm continuum emission, overlaid onto an optical image extracted from the Digitized Sky Survey, is shown in Fig. 4. This λ1.2 mm-map is already smoothed to a beamsize of 15″ to improve the signal-to-noise ratio.

The emission is concentrated along a narrow ridge which follows closely the dusty optical disk, but is less extended, perhaps because of the sensitivity limit of our data. Although the emission is enhanced near the centre, there is no evidence for a nuclear point source. Several local maxima are visible along the major axis, but with some difference between the northern and the southern half. Whereas in the north there are three separate peaks at projected radii of about 1′, 2′, and 3.′5, they seem to be somehow smeared out in the southern half, except the one at $x \sim 3.'5$.

In Fig. 5 we show the λ1.2 mm continuum map, smoothed to a resolution of 21″ HPBW, together with an HI total intensity map as received from Sancisi (priv. comm.), and the positions observed in the CO lines. NGC 5907 is a really exemplary galaxy for the existence of galactic warps in neutral hydrogen (Sancisi 1976). It is, moreover, the first "normal" galaxy where a warp in the outer disk was observed. But in contrast to NGC 4565, another normal edge-on galaxy recently observed at λ1.2 mm (Neininger et al. 1996), no indication for a warp of the thermal dust emission can be seen (although the northernmost peak seems to be slightly shifted westwards with respect to the major axis). This may of course be due to the decreasing sensitivity at the outer edges of our dust map, which we reach at radii of $\sim 300''$, where the HI-warp is only marginally detected.

4.2. ISM distributions along the major axis

Fig. 6 shows the distribution of the λ 1.2 mm continuum emission along the major axis, together with the line intensities of the ^{12}CO(1 − 0) and the HI emission. The spatial resolution of all three data sets is 21″, as given by the ^{12}CO(1 − 0) data.

The continuum emission shows (more clearly in this plot than in the maps) the existence of two bright maxima at the end of the emission ridge ($x \sim \pm 200''$) and of two less pronounced ones at $x \sim \pm 120''$, even if the southeastern one seems to be smeared out. Besides these similarities between the northern and the southern half the distribution is slightly asymmetric on smaller scales. The emission is detected up to radii of $\sim 250''$ in the south and even further, up to $\sim 280''$, in the northern half (with a significance of 2 σ). Since there is λ 1.2 mm continuum emission beyond the edge of the CO disk, dust associated with the atomic component makes a significant contribution to the 1.2 mm flux.

The distribution of the CO line-intensities (and therefore the column densities of the molecular gas) shows also a maximum in the central region and decreases with increasing distance from the centre. Two further maxima are apparent at $x \sim \pm 120''$. These features may be due to molecular rings and/or spiral arms in the inner part of the disk.

The HI distribution shows a different behaviour. It has a minimum near the centre, increases at $x \leq 80''$, stays then roughly constant with several local peaks up to $x \sim \pm 200''$, and drops again further outwards. Hence this component is much more extended than the molecular gas in this galaxy.

If we compare the dust emission with both gas phases, we find that it correlates with the molecular gas in the inner part of

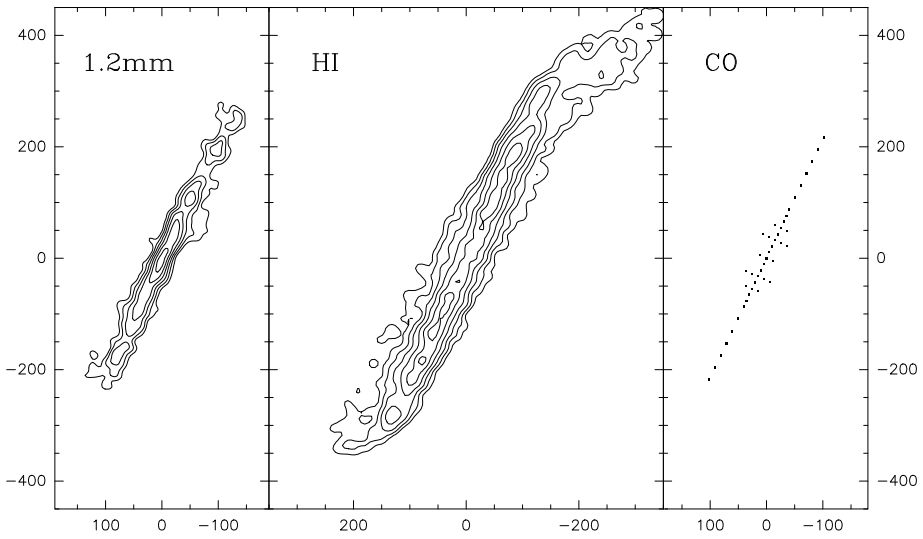

Fig. 5. Contour maps of the $\lambda 1.2$ mm continuum emission (left) and the HI line emission (middle), as well as positions observed in the CO lines (right), all at the same scale and aligned in declination. The spatial resolution of the two maps is $21''$. Contour levels are 3, 7, 12, 18, 25, 33 mJy/beam area for the $\lambda 1.2$ mm map and 8, 15, 25, 40, 55, 7010^{20} atoms cm^{-2} for the HI map

the disk. At large radii, on the other hand, where CO is no longer detected, it seems to follow the HI emission. This result confirms qualitatively that for NGC 4565 of Neininger et al. (1996). At smaller scales, we find the two outer peaks in the dust emission at $x \sim \pm 200''$ corresponding to local maxima in the HI distribution, although there is a small displacement, especially on the southeastern side. From both CO peaks at $x \sim \pm 120''$ only the northwestern one has a clear counterpart in the dust distribution, whereas in the southeastern half the dust emission shows just a small enhancement at this radius.

4.3. Disk thickness

García-Burillo et al. (1997) estimated from their Plateau de Bure observations of the central region of NGC 5907 an inclination of 86.5° and a thickness of the molecular disk of $\leq 3''$. In order to check if this is in agreement with our observations, we fitted the observed z-distribution (the averaged spectra are shown in Fig. 7) with a Gaussian profile. Using the beamwidths given in Sect. 2.1 we determined a deconvolved thickness (FWHM) of the CO emission ridge of $(13 \pm 5)''$, somewhat thicker than in NGC 4565 (Neininger et al. 1996). Additional off-axis observations at $x = 60''$ have shown that this apparent thickness is nearly constant along the major axis. In order to estimate the extent of the atomic gas and the thermal dust emission perpendicular to the plane, we performed cuts along the minor axis of both maps. These lead to a mean beam deconvolved FWHM of the emission of $(47 \pm 4)''$ for the HI and $(16 \pm 4)''$ for the $\lambda 1.2$ mm emission.

Since the galaxy is not perfectly seen edge-on, but under an inclination of $i = 86.5°$, a particular fraction of the off-axis emission is just projected from large radii to large z. We modelled this emission, using the radial CO profile obtained in Sect. 3.2 and a similar model, consisting of three rings, for the HI emission. The best agreement between model and data is found for a disk with a thickness (FWHM) of $8''$ (which corresponds to $\sim$ 400 pc) for the CO and of $28''$ ($\sim$ 1.5 kpc) for the HI. Both values seem to be unexpectedly large for a non-interacting spiral with only moderate star forming activity.

We should note, however, that it is difficult to account for a warp in this simple modelling, and the results are very sensitive to the exact values of the inclination and the telescope beamwidth. Therefore, due to the large uncertainties, a thin molecular disk cannot be ruled out.

4.4. Dust properties

4.4.1. Non-dust contributions to the observed flux

Using a ring integration method, we have determined the total flux density at $\lambda 1.2$ mm and found $S_{1.2\mathrm{mm}} = 605 \pm 55$ mJy. This value, however, cannot be attributed to thermal dust radiation alone. The broad band emission measured with the bolometer at 245 GHz rather consists of several components: thermal dust emission, free-free radiation, synchrotron radiation, and the CO$(2-1)$ and some weaker lines. Since we are mainly interested in the first, we have to determine the contributions due to the other processes and to subtract them.

The contribution of the ^{12}CO$(2-1)$ line to the surface brightness measured with the bolometer can be calculated through

$$F_{\mathrm{line}} = \frac{2k\nu^3c^{-3}}{\Delta\nu_{\mathrm{bol}}}\,\Omega_{\mathrm{beam}}\,I_{\mathrm{CO}(2-1)} \approx 0.058\,I_{\mathrm{CO}(2-1)} \quad (1)$$

(with $I_{\mathrm{CO}(2-1)} = \int\limits_{\mathrm{line}} T_{\mathrm{mb}}(^{12}\mathrm{CO}(2-1))\,dv$ in Kkms^{-1}) for a bolometer bandwidth of 70 GHz and a beamwidth of $11''$ for the continuum observations. With an assumed contribution of other isotopes and lines from other molecules of about 10 % of ^{12}CO we estimate a total flux density due to line contributions of $S_{\mathrm{line}} = 52 \pm 4$ mJy.

The contribution of the continuum emission due to thermal and relativistic electrons is more difficult to determine since the

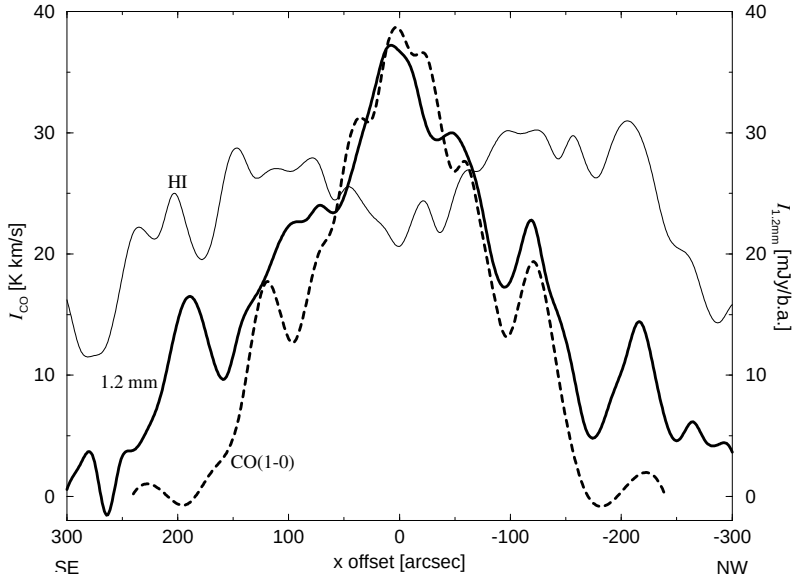

Fig. 6. The distribution of the ^{12}CO$(1-0)$ (thick dashed line, left scale) and the $\lambda 1.2$ mm continuum (thick solid line, right scale) along the major axis of NGC 5907. The HI distribution (thin solid line, arbitrary units) is also shown. The spatial resolution in all three curves is $21''$

radio continuum flux density at $\nu = 1 - 10$ GHz originates partly in a double background source in the southern half of the galaxy (Hummel et al. 1984; Dumke et al. 1995). Furthermore the spectral behaviour of this background source is unknown, and the fraction of the galaxies' thermal emission is difficult to estimate. We used a total flux density of 47 ± 5 mJy at a frequency of 10.55 GHz as derived by Dumke et al. (1995), a thermal fraction of 30 % at this frequency and a nonthermal spectral index of -0.85 which are typical for spiral galaxies (Niklas et al. 1997) to calculate a value of $S_{\rm sync+ff} = 13 \pm 4$ mJy at 245 GHz, which is about 2 % of the total flux density.

Besides these integrated values, we had to estimate the non-dust contributions along the major axis. The fraction of the CO lines, i.e. the line-to-continuum ratio, was calculated for each position from the CO$(2-1)$ line following Eq. 1 and subtracted. Again we assumed that a fraction of 10 % of the ^{12}CO$(2-1)$-line stems from other lines in the bolometer band. For the free-free and synchrotron emission, we subtracted a fraction of 2 % at each position, in accordance with the value estimated above.

4.4.2. Dust temperatures

After subtracting the contributions of molecular lines and of synchrotron and free-free radiation, we determined a total flux density at 245 GHz due to thermal dust emission of

$$S_{\rm dust} = 540 \pm 60 \,{\rm mJy} \ .$$

Including published IRAS flux densities (Young et al. 1989) our observations allow to estimate color temperatures for the dust. We fitted a two-component modified Planck function to the data, using the points from 25 μm to 1.2 mm and under the assumption of a dust spectral index of 2 (e.g. Chini et al. 1986).

The observed spectrum and the fitted curves (as well as their sum) are shown in Fig. 8. The estimated temperatures for the two components to which we refer as cold and warm dust are 18 K and 54 K respectively. This result shows that cold

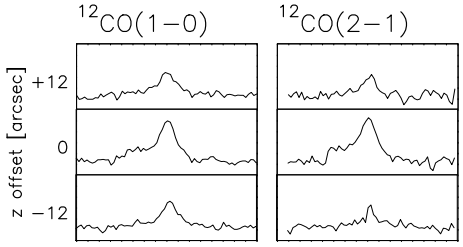

Fig. 7. Averaged ^{12}CO$(1-0)$ and $(2-1)$ spectra of the cuts through the centre. The portion of the spectra shown in each box ranges from $v_{\rm hel} = 300\,{\rm km/s}$ to $v_{\rm hel} = 1000\,{\rm km/s}$ and from $T_{\rm mb} = -0.1$ K to $T_{\rm mb} = 0.4$ K

dust is necessary to explain the thermal continuum emission at $\lambda 1.2$ mm. The warmer dust alone which can be detected in the far-infrared by IRAS is not sufficient to account for the strong mm-emission and to explain our data.

Although NGC 5907 is a relatively inactive galaxy which does not show any signs of remarkable star forming activity (e.g. Dumke et al. 1995), the dust emission is slightly enhanced at smaller galactocentric radii, and the dust may be somewhat warmer in this region. The FIR emission of NGC 5907 was mapped by Wainscoat et al. (1987), using the IRAS CPC instrument, at $\lambda\lambda$ 50 and 100 μm with a resolution of $75''$ and $89''$ respectively. These maps were used to obtain spectra at different positions along the major axis of NGC 5907. We found that the temperature of the cold dust is somewhat higher in the central region (~ 20 K) than the value we got from the integrated flux densities, and drops to ~ 16 K at the outer disk. A similar decrease is also found for other normal disk galaxies like NGC 891 (Guélin et al. 1993), NGC 4565 (Neininger et al. 1996), or our Milky Way (Cox & Mezger 1989).

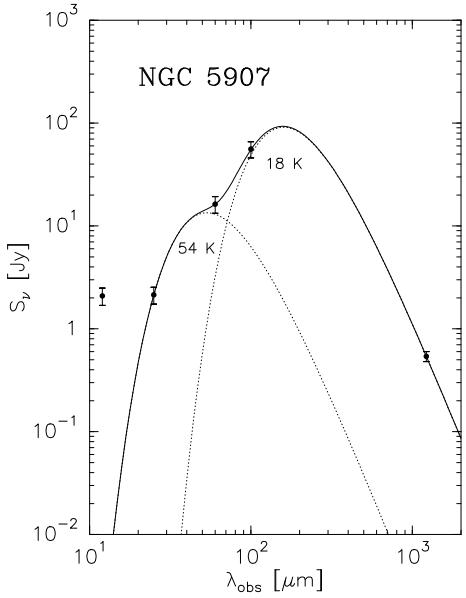

Fig. 8. Total flux density spectrum of NGC 5907 fitted by a two-component model. The data points represent IRAS flux densities (Young et al. 1989) and our bolometer observations. The dotted lines show the fitted spectra for the individual temperature components, the solid line the sum of them

4.4.3. Dust absorption cross sections

Once we have removed the contributions to the $\lambda 1.2$ mm continuum emission which are not due to cold dust, we can estimate the dust absorption cross section per hydrogen atom.

The flux density per beam emitted by a cloud (molecular or atomic) is given by

$$S_\nu = \Omega_{\rm beam} B_\nu(T_{\rm d})(1 - e^{-\tau_\lambda}) \quad (2)$$

with $\tau_\lambda = \sigma_\lambda^{\rm H} N_{\rm H}$, where $\sigma_\lambda^{\rm H}$ is the dust absorption cross section per hydrogen atom and $N_{\rm H}$ the beam-averaged hydrogen column density. Since $\tau_\lambda \ll 1$ at $\lambda 1.2$ mm, and under the assumption that the thermal dust emission comes only from matter in the neutral gas, we can express the cross section by (see Mezger et al. 1990)

$$\sigma_\lambda^{\rm H} = \frac{\lambda^2}{\Omega_{\rm beam}\, 2kT_{\rm d}} \frac{(e^x - 1)}{x} \frac{S_\nu}{N_{\rm H}} , \quad (3)$$

with $x = h\nu/kT_{\rm d}$ and $N_{\rm H} = N({\rm HI}) + 2\,N({\rm H_2})$.

In a first step we use this equation to estimate the cross-sections at radii where no molecular line emission is detected and we have to consider only the contribution from the atomic gas. The values for N(HI) are taken from the HI map shown in Fig. 5. For this calculation we use a dust temperature of $T_{\rm d}$ = 16 K since this value seems to be most appropriate for radii larger than 200″. The result is

$$\sigma_\lambda^{\rm HI} = (4.5 \pm 1.5) 10^{-27}\,{\rm cm}^2 .$$

Taking into account the grain composition of the dust and the metallicity, we can use a formulation following Mezger et al. (1990),

$$\sigma_\lambda^{\rm H} = C\, \lambda_{\rm mm}^{-2}\, b\, Z/Z_\odot . \quad (4)$$

$C = 7 \cdot 10^{-27}$ cm^2 is the dust absorption cross section at $\lambda 1$ mm following from the theoretical curves of Draine & Lee (1984), $\lambda_{\rm mm}$ the wavelength in mm, Z the metallicity, and b an empirically determined factor which accounts for the differences between Draine & Lee's grain mixtures and real grains. This parameter is adjusted to reproduce absorption cross section estimates in the FIR and is usually assumed to vary between 1 and 3. b = 1 applies to dust in the diffuse interstellar HI gas, and may also serve as a lower limit for molecular clouds. Other authors used b = 1.9 for dust embedded in molecular gas of moderate density. Recent measurements of Goldsmith et al. (1995) in nearby molecular clouds yield b = 1.5, and Pajot et al. (1986) came to a similar value. Therefore we use b = 1.5 for all calculations throughout this paper. In any case, the chosen value for b does not change our results qualitatively.

Since one expects $Z/Z_\odot \lesssim 1$ for diffuse HI clouds at a galactocentric radius of $10 - 15$ kpc in a Sc-galaxy, our value of $\sigma_\lambda^{\rm HI}$ is very close to that predicted by Draine & Lee (1984). It is also in excellent agreement with the values estimated for other nearby spiral galaxies (e.g. Neininger et al. 1996).

In a second step we use the absorption cross section $\sigma_\lambda^{\rm HI}$ estimated above and calculate the dust emission which is due to particles embedded in atomic hydrogen along the whole major axis. Therefore we take this value as an average over the radii at which hydrogen exists mainly in form of HI. The resulting amount is subtracted from the dust emission (as it was done for the non-dust contributions before). What is left must be due to dust grains embedded in clouds of molecular hydrogen, and this can be used as described in the following paragraph.

4.5. The conversion factor X and its radial variation

We continue with a third step where we make use of the radial distribution of the CO intensity and the expected radial variation of the metallicity – and therefore the absorption cross section – to estimate the column densities of the molecular hydrogen and the conversion factor X at different radii.

We take the deprojected CO intensity distribution obtained in Sect. 3.2 and calculate the corresponding radial $N({\rm H_2})$ distribution, using a conversion ratio which varies along the radius as $\log X = k_1 + k_2\, r$ with k_1 and k_2 as free parameters which have to be fitted. This exponential behaviour of X with radius was found by other authors for our galaxy (e.g. Arimoto et al. 1996). With $N({\rm H_2})$, we calculate the radial distribution of the dust emission using Eq. 3. In this calculation we assume a decrease of the dust temperature with radius from (20 ± 1.5) K in the centre to (16 ± 1.5) K at $r = 4'$, and the shallow radial metallicity distribution

$$\log \frac{Z}{Z_\odot} = (0.3 \pm 0.1) - (0.033 \pm 0.006) \frac{r}{\rm kpc} , \quad (5)$$

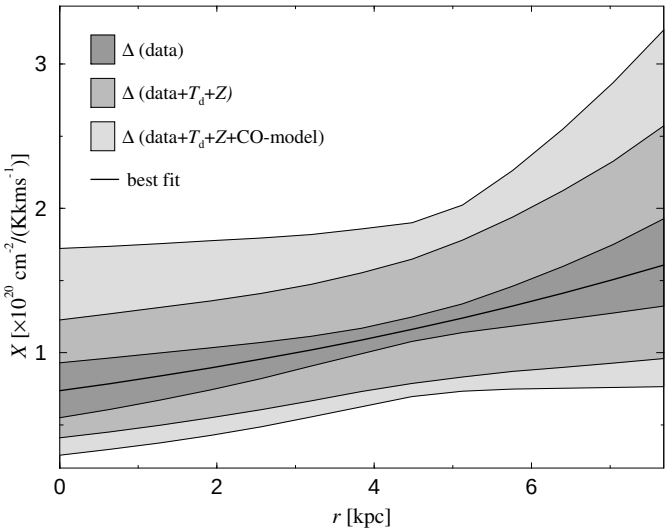

Fig. 9. Radial variation of the CO-H_2-conversion factor X in NGC 5907 as obtained from the bolometer data. The thick line shows the best fit, the different greyscales the range of possible solutions considering the uncertainties in the different input parameters. See text for details

which is an average for Sc galaxies and follows from the results of Vila-Costas & Edmunds (1992). This radial intensity distribution is then projected along the major axis and compared to the observed distribution (minus non-dust and HI contributions) by a least-squares-fit with k_1 and k_2 (see above) as free parameters.

This fit, which is restricted to $|x| \leq 150''$ (~ 7.5 kpc) to yield a higher significance, leads to the following radial variation of the X-factor:

$$\log X^* = (-0.13 \pm 0.24) + (0.044 \pm 0.024)\,\frac{r}{\mathrm{kpc}}\ , \qquad (6)$$

where $X^* = N_{\mathrm{H2}}/I_{\mathrm{CO(1-0)}}\,10^{-20}\,\mathrm{K\,km\,s^{-1}/cm^{-2}}$. The result is plotted in Fig. 9: The conversion factor is clearly below the "standard" value of $X^* = 2.3$ (Strong et al. 1988) in the whole radial range considered here. We find X^* starting from ~ 0.7 in the centre and increasing with galactocentric radius by a factor of more than 2 up to $r = 7.5$ kpc, and in all probability even more further out.

This increase of X with galactocentric radius is also found for our galaxy by Sodroski et al. (1995), using recent DIRBE results from the COBE satellite. Arimoto et al. (1996) came to the same result for the Milky Way and nearby spirals, using a method based on CO intensities and virial cloud masses.

The mentioned errors contain the statistical uncertainties in the bolometer and the HI distributions (Δdata), the dust temperature (ΔT_{d}), the metallicity (ΔZ), and the radial CO distribution (ΔCO-model). The numerical error values in Eq. 6 are estimated by varying the single input parameters, keeping the other parameters fixed. In fact the range of possible solutions is a confidence ellipsoid in a multi-dimensional parameter space.

The variation of the conversion factor with radius obviously has some effect on the estimated amount of molecular gas in galaxies. Since usually most of the CO emission is detected at smaller galactocentric radii where the conversion factor is rather small, one easily overestimates the gas mass using the "standard" value for X. On the other hand there may be large amounts of molecular hydrogen in the outer parts of galactic disks where we detect only weak CO emission.

4.6. The gas content of NGC 5907

Using the CO-H_2-conversion ratio of Strong et al. (1988), $X = 2.3\ 10^{20}\mathrm{cm^{-2}/(K\,km\,s^{-1})}$, we found a molecular mass for the major axis strip of NGC 5907 of $M_{\mathrm{H2}} = (1.0 \pm 0.2)\ 10^9\ M_\odot$. Assuming that the extent of the CO emission in z-direction, as measured with our cuts through the center, is constant along the major axis, we estimate a total molecular mass of $M_{\mathrm{H2}} = (1.9 \pm 0.3)\,10^9\ M_\odot$. As we have seen, the "real" X-value seems to be well below this standard value in the inner part of the galaxy, where the major fraction of CO emission is detected. Once we have an idea about the radial variation of the X-factor, we make use of the radial CO intensity as modelled in Sect. 3.2 to calculate the corresponding distribution of the column densities $N(\mathrm{H_2})$. With this method we get a molecular mass on the major axis strip of $M_{\mathrm{H2}} = (0.5 \pm 0.2)\ 10^9\ M_\odot$. which leads to a total value (for the whole galaxy) of $M_{\mathrm{H2}} = (0.9 \pm 0.3)\ 10^9\ M_\odot$.

The amount of atomic hydrogen can be estimated from an HI line flux of $S_{\mathrm{HI}} = (240 \pm 20)\,\mathrm{Jy\,km\,s^{-1}}$ (Huchtmeier & Richter 1989, and references cited therein) to $M_{\mathrm{HI}} = (6.9 \pm 0.6)\ 10^9\ M_\odot$. Using these values we calculate a total hydrogen mass of $M_{\mathrm{tot}}(\mathrm{H}) = (7.8 \pm 0.7)\ 10^9\ M_\odot$.

5. Comparison with other edge-on galaxies

In this section the results we obtained from the present study of NGC 5907 are compared with the Milky Way and two other edge-on galaxies already observed at $\lambda 1.2$ mm and in the CO emission, namely NGC 891 and NGC 4565. The reason why we restrict ourselves here to these few galaxies is that they have not too different properties (i.e. Hubble type, star formation, interaction state) and the analyses are based on comparable data sets. The data that correspond to this section are collected in Table 2. NGC 891, NGC 4565, and the Milky Way have already been compared in a similar way by Neininger et al. (1996).

5.1. Molecular gas distribution

One similarity between the galaxies is that the molecular gas distributions (as traced by the CO intensity) all show a central peak and a ring with a radius of $3-5$ kpc. But the ratio $I_{\mathrm{ring}}/I_{\mathrm{peak}}$ in the major axis intensity distribution differs from galaxy to galaxy. The Sb galaxy NGC 4565 has a relatively strong ring compared to the central peak, in the Sbc galaxy NGC 891 it is less pronounced, and in the Sc galaxy NGC 5907 it is just marginal detectable. Whether this variation is due to the different Hubble types or occurs just by chance, is not known yet. Since galaxies of later Hubble types in general tend to have flatter

Table 2. Dust and gas parameters of several edge-on galaxies and the Milky Way in comparison

	NGC 891	NGC 4565	NGC 5907	Milky Way *
General:				
Distance [Mpc]	9.6	10.0	11.0	–
Inclination	89°	87°	86°.5	–
Hubble Type	Sbc	Sb	Sc	Sb
Opt. Diameter D_{25} [kpc]	37.7	47.1	39.4	–
Dust temperatures:				
$T_{\rm d}$(center) [K]	≤ 20	18	20	19
$T_{\rm d}$(disk) [K]	15	15	16	17
Masses:				
$M_{\rm HI}$ [$\times 10^9\,M_\odot$]	3.7	6.0	6.9	4.8
$M_{\rm H2}$ [$\times 10^9\,M_\odot$]	4.8† 1.8‡	1.5† 0.6‡	1.9† 0.9‡	1.0†
Molecular gas distribution:				
$I_{\rm ring}/I_{\rm peak}$	medium	large	small	–
FWHM $\perp$ plane [kpc]	0.3(thin disk)	0.3	0.4	0.2
Kinematics:				
$v_{\rm sys}$ [km s^{-1}]	535	1230	677	–
$v_{\rm term}$ [km s^{-1}]	225	255	230	220
$R_{\rm turnover}$ [kpc]	5.5	4.2	3.0	5.0
$v_{\rm Bar}$ [km s^{-1}]	250	150	200	260
FIR & Activity:				
$L_{\rm FIR}$ [$\times 10^{10}\,L_\odot$]	1.31	0.28	0.44	–
$L_{\rm IR(tot)}$ [$\times 10^{10}\,L_\odot$]	1.93	0.48	0.75	–
$SFE = \frac{L_{\rm IR(tot)}}{M_{\rm H2}}$ [$L_\odot\,M_\odot^{-1}$]†	4.0	3.2	3.9	–

* for $R_\odot$ = 10 kpc
† as derived from CO
‡ as derived from λ1.2 mm (using b = 1.5 – see Sect. 4.4.3)

References: this work, or de Vaucouleurs et al. (1991), García-Burillo et al. (1992), Guélin et al. (1993), Henderson et al. (1983), Neininger et al. (1996), Rupen (1991), Strong et al. (1988), Young et al. (1989)

rotation curves in their inner disks, there may be dynamical reasons for a less pronounced ring near the turnover radius.

A second ring-like feature in the CO distributions, which may trace a spiral arm structure, is only detected in NGC 4565 (at $r \sim 8$ kpc) and NGC 5907 (at $r \sim 7$ kpc).

5.2. Kinematics

Compared to NGC 891 and NGC 4565, the kinematics of the central regions point to NGC 5907 being somehow intermediate between these two. NGC 4565 just shows a marginal indication for a central bar (Neininger et al. 1996), whereas in NGC 891 molecular gas was detected at forbidden velocities and the kinematics in the central region could be successfully modelled by orbits driven by a bar potential (García-Burillo & Guélin 1995). NGC 5907 seems also to exhibit a central bar, but much less pronounced than NGC 891 (García-Burillo & Guélin 1995; García-Burillo et al. 1997).

5.3. Dust properties

Compared to other galaxies, the continuum emission at λ 1.2 mm of NGC 5907 is surprisingly strong. Because of the similar distances of the galaxies to be considered here, it is sufficient to compare the measured intensities. In Fig. 4 (NGC 5907) they exceed values of 24 mJy per 15″ beam (or 35 mJy per 21″ beam in a smoothed map), whereas in NGC 4565 the map maxima reach just values of about 22 mJy per 20″ beam (see Fig. 3 of Neininger et al. 1996). Although they did not give a value for the total flux density of NGC 4565, this seems to be much lower than in NGC 5907, too. Guélin et al. (1993) determined a value of 850 mJy for the non-interacting Sbc-galaxy NGC 891. This points also to an unexpectedly high value for NGC 5907 since the infrared emission of NGC 891 is about 3 times higher (Young et al. 1989, Table 2).

This strong thermal dust emission may be partially due to a nuclear point source which shows some characteristics of a weak starburst (Skrutskie et al. 1985). Since star formation and the subsequent supernova events always lead to enhanced turbulence in the ISM, this may be the reason for stronger beam depolarization and the non-detection – in contrast to NGC 891 and NGC 4565 – of ordered magnetic fields at λ2.8 cm (with a resolution of 69″ HPBW) by Dumke et al. (1995).

6. Summary and conclusions

We performed molecular line and λ1.2 mm bolometer observations of the edge-on galaxy NGC 5907. The important results which were concluded from that observations can be summarized as follows:

The distribution of the molecular gas (as traced by CO) shows a maximum in the central region and a ring or spiral arm structure at $r \sim 7$ kpc. Further analysis of the major axis distribution reveals a second ring at r = 3.7 kpc, near the turnover point of the rotation curve. The kinematics can be described by rigid rotation in the inner part, a turnover at 3 – 3.5 kpc, and differential rotation with a velocity of 230 km/s in the outer disk. Further a high-velocity component is present in the central region which is most probably due to a central bar.

The observed $\lambda 1.2$ mm emission is mainly due to thermal radiation of cold dust with an average temperature of $T_{\rm d} = 18$ K, with a small gradient from 20 K to 16 K from the centre to the outer disk. This cold dust component is necessary to explain our results. The warmer dust detected by IRAS is not sufficient to account for the continuum emission at $\lambda 1.2$ mm.

This dust emission follows closely the molecular gas in the central region, but is also detected at large radii, where no CO can be seen. In these regions the dust absorption cross section per H atom could be estimated to $\sigma_\lambda^{\rm HI} \sim 4.5\ 10^{-27}\,{\rm cm}^2$. Two outer maxima of the dust distribution, which correlate with similar features in the HI emission, may indicate the existence of outer spiral arms at a radius of about 11 kpc.

Because of its optical thinness the thermal continuum emission of cold dust provides an independent way to estimate hydrogen column densities. From the $\lambda 1.2$ mm emission we estimated a molecular mass of NGC 5907 of $0.9\ 10^9\,{\rm M}_\odot$, about 50 % smaller than from the CO emission. By combining the CO and continuum data we found that the CO-H_2-conversion factor increases with galactocentric radius, from $\sim 0.7\ 10^{20}$ at the centre to $\sim 1.6\ 10^{20}\,{\rm cm}^{-2}/{\rm K\,km\,s}^{-1}$ at $r = 7.5$ kpc.

The comparison of our results concerning gas distribution, kinematics and dust properties lead to some similarities between NGC 5907 and other edge-on galaxies. NGC 5907 seems to be intermediate between the other galaxies in respect of some properties (central kinematics, $\lambda 1.2$ mm intensities), probably because of its intermediate star formation.

Acknowledgements. We wish to thank Fabrice Herpin for his collaboration during the CO observations and Renzo Sancisi for making a contour map of the total HI emission available to us. Further we acknowledge the use of software written by Endrik Krügel.

References

Arimoto N., Sofue Y., Tsujimoto T., 1996, PASJ 48, 275
Barnaby D., Thronson H.A.Jr., 1992, AJ 103, 41
Braine J., Krügel E., Sievers A., Wielebinski R., 1995, A&A 295, L55
Braine J., Guélin M., Dumke M., et al., 1997, A&A (submitted)
Casertano S., 1983, MNRAS 203, 735
Chini R., Krügel E., Kreysa E., 1986, A&A 167, 315
Combes F., 1991, ARA&A 29, 195
Cox P., Mezger P.G., 1989, A&AR 1, 49
Dahlem M., Lisenfeld U., Golla G., 1995, ApJ 444, 119
de Vaucouleurs G., de Vaucouleurs A., Corwin H.G., et al., 1991, Third Reference Catalogue of Bright Galaxies. Springer-Verlag, New York
Draine B.T., Lee H.M., 1984, ApJ 285, 89
Dumke M., Krause M., Wielebinski R., Klein U., 1995, A&A 302, 691
García-Burillo S., Guélin M., 1995, A&A 299,657
García-Burillo S., Guélin M., Cernicharo J., Dahlem M., 1992, A&A 266, 21
García-Burillo S., Guélin M., Neininger N., 1997, A&A (in press)
Goldsmith P.F., Bergin E.A., Lis D.C., 1996, in: Latter W.B. et al. (eds.), CO: Twenty-five Years of Millimeter-wave Spectroscopy, Proc. IAU Symp. 170. Kluwer, Dordrecht
Guélin M., Sancisi R., Weliachew L., van Woerden H., 1974, in: Weliachew L. (ed.), Dynamics of Spiral Galaxies, 291. Colloque C.N.R.S. 241, Editions du CNRS
Guélin M., Zylka R., Mezger P.G., Haslam C.G.T., Kreysa E., 1995, A&A 298, L29
Guélin M., Zylka R., Mezger P.G., Haslam C.G.T., Kreysa E., Lemke R., Sievers A., 1993, A&A 279, L37
Henderson A.P., Jackson P.D., Kerr F.J., 1983, ApJ 263, 116
Hildebrand R.H., 1983, QJRAS 24, 267
Huchtmeier W.K., Richter O.-G., 1989, A general catalogue of HI observations of galaxies. Springer-Verlag, New York
Hummel E., Sancisi R., Ekers R., 1984, A&A 133, 1
Maloney P., Black J.H., 1988, ApJ 325, 389
Mezger P.G., Wink J.E., Zylka R., 1990, A&A 228, 95
Neininger N., Guélin M., García-Burillo S., Zylka R., Wielebinski R., 1996, A&A 310, 725
Niklas S., Klein U., Wielebinski R., 1997, A&A (in press)
Pajot F., Boissé P., Gispert R., et al., 1986, A&A 157, 393
Rupen M.P., 1991, AJ 102, 48
Sancisi R., 1976, A&A 53, 159
Sasaki T., 1987, PASJ 39, 849
Sievers A.W., Reuter H.-P., Haslam C.G.T., Kreysa E., Lemke R., 1994, A&A 281, 681
Skrutskie M.F., Shure M.A., Beckwith S., 1985, ApJ 299, 303
Sodroski T.J., Odegard N., Dwek E., et al., 1995, ApJ 452, 262
Sofue Y., 1994, PASJ 46,173
Strong A.W., Bloemen J.B.G.M., Dame T.M., et al., 1988, A&A 207, 1
Vila-Costas M.B., Edmunds M.G., 1992, MNRAS 259, 121
Wainscoat R.J., de Jong T., Wesselius P.R., 1987, A&A 181, 225
Young J.S., Xie S., Kenney J.D.P., Rice W.L., 1989, ApJS 70, 699
Zylka R., 1996, "Pocket Cookbook" for the MOPS Software. MPIfR, Bonn

This article was processed by the author using Springer-Verlag LaTeX A&A style file *L-AA* version 3.